PAPER

A comparative study of high-pressure behaviors of the two polymorphs of $Ho_2Ge_2O_7$

Hui Li, [ID] [ac] Nana Li,[b] Pinwen Zhu*[cd] and Xin Wang*[cd]

Two polymorphs of polycrystalline $Ho_2Ge_2O_7$, one with tetragonal structure and the other with cubic structure, were synthesized by using different methods. The structural stabilities of these two polymorphs under high pressure were investigated by angle-dispersive X-ray diffraction (ADXRD). Pressure-induced amorphization was found in the tetragonal $Ho_2Ge_2O_7$, which is suggested to be associated with the breaking-up of long chains of the edge-shared polyhedron group Ho_4O_{20}. By contrast, cubic $Ho_2Ge_2O_7$ is stable at high pressures up to 33.3 GPa.

1. Introduction

Spin ice has proven to be one of the most fruitful marriages of theoretical and experimental condensed matter physics.[1–4] It is a remarkable magnetic ground state that can arise in geometrically frustrated pyrochlores, $A_2B_2O_7$, when magnetic rare-earth ions are situated on the vertices of a lattice of corner-sharing tetrahedra. Competing nearest-neighbor and long-range dipolar interactions result in a short-range ordered ground state for each tetrahedron in which two spins point in and two spins point out.[5] The spin-ice state was first observed in $Ho_2Ti_2O_7$ by Harris *et al.* in 1997;[6] since that time, spin ices have been a subject of active experimentation, allowing theorists to come a long way towards understanding this remarkable ground state. Despite significant interest in this class of compounds, only a handful of spin-ice materials have been discovered to date, including the titanates $A_2Ti_2O_7$,[6–8] the stannates $A_2Sn_2O_7$ [9,10] and, more recently, the germanates $A_2Ge_2O_7$.[11,12] Recently, the observation of emergent monopole excitations which have captured the attention of the broader scientific community have made spin-ice materials more intriguing.[13–18] $Ho_2Ge_2O_7$, a member of the rare-earth pyrogermanate series $A_2Ge_2O_7$, has been attracting extensive interest because it was found to be a new highly correlated spin-ice material with the highest density of monopoles in the Ho series at low temperatures, and the best natural candidate for monopole studies.[19]

From a structural point of view, rare-earth pyrogermanates $A_2Ge_2O_7$ possess a variety of crystal structures under ambient conditions, such as triclinic phase for Ln = La, Pr, Nd–Gd,

tetragonal phase for Ln = Gd–Lu, and monoclinic phase for $In_2Ge_2O_7$ and $Sc_2Ge_2O_7$. Moreover, depending on the synthesis method, different structural modifications of $Ln_2Ge_2O_7$ can be obtained. By conventional solid state synthesis, $Ho_2Ge_2O_7$ has the tetragonal structure. However, the cubic phase of $Ho_2Ge_2O_7$ can be synthesized by the high-pressure and high-temperature (HPHT) method. Therefore, pressure is an important weapon in a researcher's arsenal for exploring phase space. Pressure is also used to drive materials into new electronic states. Under high pressure, some materials become superconductors, others undergo magnetic phase transitions, and others undergo metal–insulator phase transitions.[20,21] In magnetic pyrochlore oxides, pressure has been shown to freeze the spin-liquid ground state of $Tb_2Ti_2O_7$.[22] So, studies on the stability of $Ho_2Ge_2O_7$ under high pressure are particularly important to understand its exotic magnetic phenomenon.

In this work, we successfully synthesized the two types of $Ho_2Ge_2O_7$ using different methods. The structural stabilities of these two polymorphs of $Ho_2Ge_2O_7$ were investigated by angle-dispersive synchrotron X-ray powder diffraction (ADXRD) at high pressures. Pressure-induced amorphization was found in the tetragonal $Ho_2Ge_2O_7$. Meanwhile, the cubic $Ho_2Ge_2O_7$ was stable up to the highest pressure tested.

2. Experimental section

Synthesis

The tetragonal $Ho_2Ge_2O_7$ was synthesized by standard solid state reaction method. High purity oxides of Ho_2O_3 (99.99%, powder) and GeO_2 (99.99%, powder) were used as the starting materials. The raw materials with nominal compositions of $Ho_2Ge_2O_7$ were uniformly mixed in an agate mortar. The powder obtained was pressed into small pellets and then calcined at 1373 K in air for 12 h. The cubic $Ho_2Ge_2O_7$ was synthesized by the HPHT method. The as-prepared powders were loaded into a cubic anvil HPHT apparatus (SPD-6 × 600) at

[a] College of Science, Guangxi University for Nationalities, Nanning, 530006, China
[b] Center for High Pressure Science and Technology Advanced Research, Shanghai 201203, China
[c] State Key Laboratory of Superhard Materials, Jilin University, Changchun 130012, China. E-mail: xin_wang@jlu.edu.cn; zhupw@jlu.edu.cn
[d] College of Physics, Jilin University, Changchun 130012, China

a temperature of 1573 K and a pressure of 5.2 GPa with a holding time of 15 min.

Characterization

Under ambient conditions, the crystal phase structures of the synthesized samples were characterized by X-ray powder diffraction (XRD) using a Rigaku D/max-2500 with Cu Kα radiation ($\lambda = 1.54056$ Å) in the range 2θ from 10° to 90° at a scanning rate of 4° min^{-1}. The high-pressure angle-dispersive XRD patterns for the two types of Ho$_2$Ge$_2$O$_7$ were collected at beamline 4W2 of the Beijing Synchrotron Radiation Facility, using a monochromatic wavelength of 0.6199 Å. A diamond-anvil cell (DAC) was utilized to generate high pressure, using a T301 stainless steel gasket which was pre-indented to 50 μm thickness. One piece of the as-prepared samples, a small piece of ruby as the pressure calibrant[23] and a 16 : 3 : 1 methanol/ethanol/water mixture as pressure-transmitting medium were loaded into the diamond-anvil cells. The experimental parameters, including the distance between sample and detector, were calibrated using CeO$_2$ standard reference material. FIT2D software was employed to convert the image plate records into intensity *versus* diffraction angle 2θ patterns. Rietveld analyses were performed with the software GSAS.[24] The refinement parameters were the lattice constants, the atomic position of oxygen, a Chebyshev polynomial background, pseudo-Voigt profile parameters, a common isotropic thermal parameter for all atom sites and an overall intensity scaling factor.

3. Results and discussion

Crystal structures under ambient conditions

The observed and calculated XRD patterns of the two types of Ho$_2$Ge$_2$O$_7$ together with their differences are shown in Fig. 1. The diffraction peaks in Fig. 1a match well with the tetragonal structure Ho$_2$Ge$_2$O$_7$ (S.G. $P4_12_12$, no. 92) and the obtained cell parameters are: $a = b = 6.8041(1)$ Å, $c = 12.3734(1)$ Å, $V =$
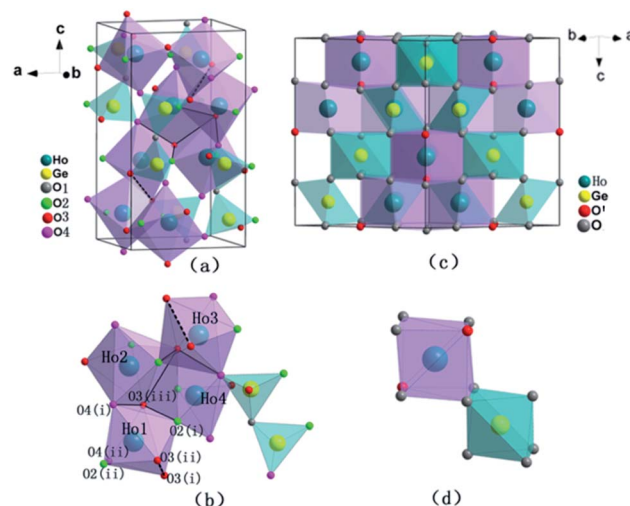

Fig. 2 Schematic representation of the crystal structures of the tetragonal Ho$_2$Ge$_2$O$_7$ ((a) and (b)) and the cubic Ho$_2$Ge$_2$O$_7$ ((c) and (d)).

572.83(1) Å^3 with $Z = 4$. In this kind of crystal structure, each Ho^{3+} ion is coordinated to seven oxygen atoms. The Ge$_2$O$_7$ unit consists of two tetrahedra (GeO$_4$) joined by a bridging oxygen atom. The bridging oxygen atoms of the Ge$_2$O$_7$ unit do not coordinate to the Ho^{3+} ion. The coordination polyhedron of the Ho^{3+} ion is a distorted pentagonal bipyramid with the Ho^{3+} ion located nearly in the basal plane. The pentagonal axis is almost parallel to the crystal c-axis. Each HoO$_7$ polyhedron shares three of its O–O edges with neighboring polyhedra. Schematic illustrations are shown in Fig. 2a and b.

The crystal structure data of the cubic Ho$_2$Ge$_2$O$_7$ were refined by Rietveld analysis of the X-ray powder diffraction data. The

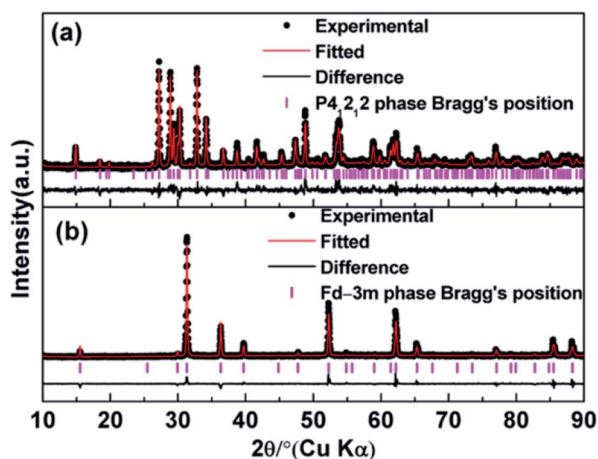Fig. 1 Observed, calculated and difference X-ray powder patterns of Ho$_2$Ge$_2$O$_7$ at ambient pressure: (a) Rietveld refinement for the tetragonal Ho$_2$Ge$_2$O$_7$ and (b) Rietveld refinement for the cubic Ho$_2$Ge$_2$O$_7$.

Table 1 The refined atomic coordinates of the cubic and tetragonal Ho$_2$Ge$_2$O$_7$ at ambient pressure

Compound	Ho$_2$Ge$_2$O$_7$	Ho$_2$Ge$_2$O$_7$
Crystal system	Cubic	Tetragonal
Space group	$Fd\bar{3}m$ (227)	$P4_12_12$ (92)
a/Å	9.8974(3)	6.8041(1)
b/Å	9.8974(3)	6.8041(1)
c/Å	9.8974(3)	12.3734(1)
Atoms	Wyckoff ($x\ y\ z$)	Wyckoff ($x\ y\ z$)
Ho	16d (0.5 0.5 0.5)	8a (0.8761(7) 0.3413(8) 0.1352(1))
Ge	16c (0 0 0)	8a (0.8857(3) 0.1469(9) 0.6199(4))
O(1)	48f (0.3255(10) 0.125 0.125)	4a (0.8141(5) 0.1859(6) 0.7500(8))
O(2)	8b (0.375 0.375 0.375)	8a (−0.0319(8) 0.1362(6) 0.6260(2))
O(3)		8a (0.0565(6) 0.3575(4) 0.5886(7))
O(4)		8a (0.6774(3) 0.1254(6) 0.5528(4))
Residuals^a/%	R_{wp}: 7.07%	R_{wp}: 5.83%
	R_p: 5.64%	R_p: 4.61%

^{a} R_{wp} and R_p as defined in GSAS.[24]

observed and calculated XRD patterns along with the difference plot are shown in Fig. 1b. The cubic $Ho_2Ge_2O_7$ belongs to the $Fd\bar{3}m$ (no. 227) space group with the lattice parameters $a = 9.8974(3)$ Å and $Z = 8$. In this cubic phase, it can be formulated as $Ho_2Ge_2O_6O'$ with the Ge ion site at 16c, Ho at 16d, O at 48f and O' at 8b. The Ho site (16d) coordination polyhedron is a distorted cube that generally contains larger cations, and the Ge site (16c) is a distorted octahedron. It is worth noting that there is only one adjustable positional parameter x for the O atom at the 48f site. Schematic illustrations of the cubic $Ho_2Ge_2O_7$ are shown in Fig. 2c and d. In addition, the refined atomic position coordinates of the two polymorphs of $Ho_2Ge_2O_7$ are given in Table 1.

Pressure-induced amorphization of the tetragonal $Ho_2Ge_2O_7$

The *in situ* XRD patterns of the tetragonal $Ho_2Ge_2O_7$ at various pressures up to 22.5 GPa were collected and a few representative patterns are shown in Fig. 3. As can be seen from Fig. 3a, the pressure-dependent X-ray data do not reveal any new diffraction peaks or peak splitting, which indicates that a typical tetragonal structure remains from ambient pressure up to 13.6 GPa. With
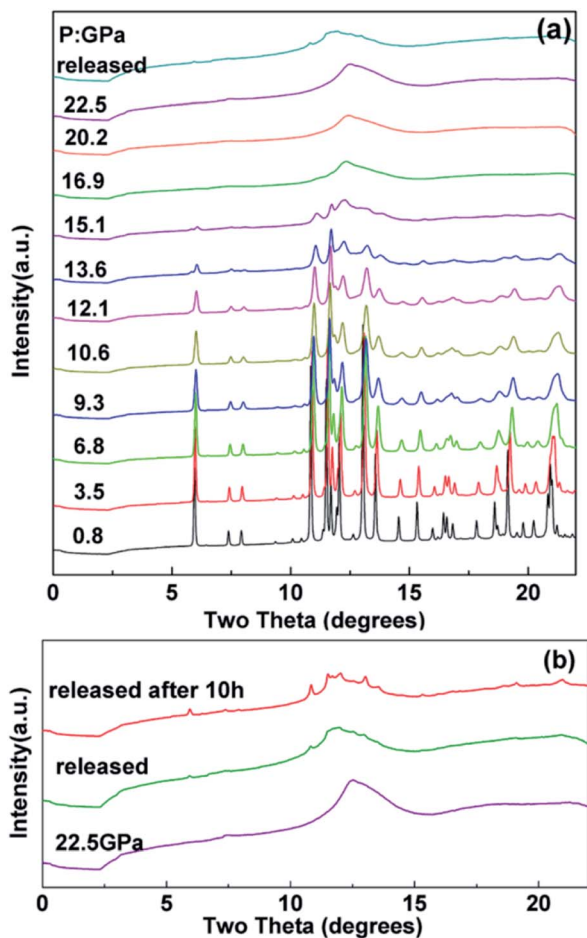
further increasing pressure, most of the sharp bands have disappeared at 16.9 GPa and no diffraction peaks can be observed, which suggests the formation of an amorphous phase. After releasing the pressure, pressure-induced amorphization of $Ho_2Ge_2O_7$ is maintained, which indicates the nonreversible nature of the phase transition. A few small peaks appeared after quenching and holding the sample under ambient conditions for 10 h. The recorded pattern for 10 h after release of pressure is almost identical to that of the original phase of tetragonal $Ho_2Ge_2O_7$, as shown in Fig. 3b.

Pressure-induced amorphization has been the subject of intense study for the past few years because of its importance in materials science and solid state physics.[25–27] A pressure-induced amorphization of α-$NaVO_3$ was observed by Raman spectroscopy, which involved the tetrahedral VO_4 chains breaking up abruptly at the transition pressure.[28] In addition, silicates and metavanadate compounds also have chain structures and are the best examples of amorphous materials.[29–31] As can be seen in Fig. 2a and b, each HoO_7 polyhedron shares three of its O–O edges with neighboring polyhedra. And we can clearly see the four polyhedra (Ho_1O_7, Ho_2O_7, Ho_3O_7, Ho_4O_7) close together. The Ho_1O_7 polyhedron and Ho_3O_7 polyhedron share an O3(i)–O3(ii) edge with the four other closest polyhedra. In the crystal structure of $Ho_2Ge_2O_7$, there is a chain, whose constituent unit (Ho_4O_{20}) is four edge-shared polyhedrons closely linked. In order to understand the reason for the amorphization, we plotted the variation of bond length with pressure for tetragonal $Ho_2Ge_2O_7$ (Fig. 4). The bond lengths of Ho–O3(i) and Ho–O3(ii) always remain longer than the other Ho–O bond distance, from ambient pressure to the highest pressure. So the infinite Ho_4O_{20} chain is relatively easy to disconnect at this junction. Pressure-induced amorphization of $Ho_2Ge_2O_7$ is suggested to be associated with the breaking-up of long chains of the edge-shared polyhedron group Ho_4O_{20}. The tetragonal $Ho_2Ge_2O_7$ showed long-range order at low magnetic fields, but its behavior was similar to spin-ice freezing in a sufficiently strong magnetic field.[32] Owing to the appearance of pressure-
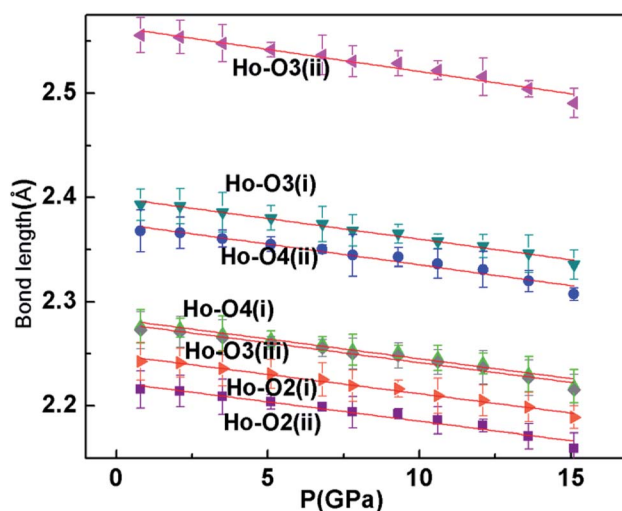

Fig. 3 (a) Representative X-ray diffraction patterns of the tetragonal $Ho_2Ge_2O_7$ at various pressures. (b) X-ray diffraction pattern for $Ho_2Ge_2O_7$ after the release of pressure.

Fig. 4 The Ho−O bond lengths in the tetragonal $Ho_2Ge_2O_7$ at various pressures.
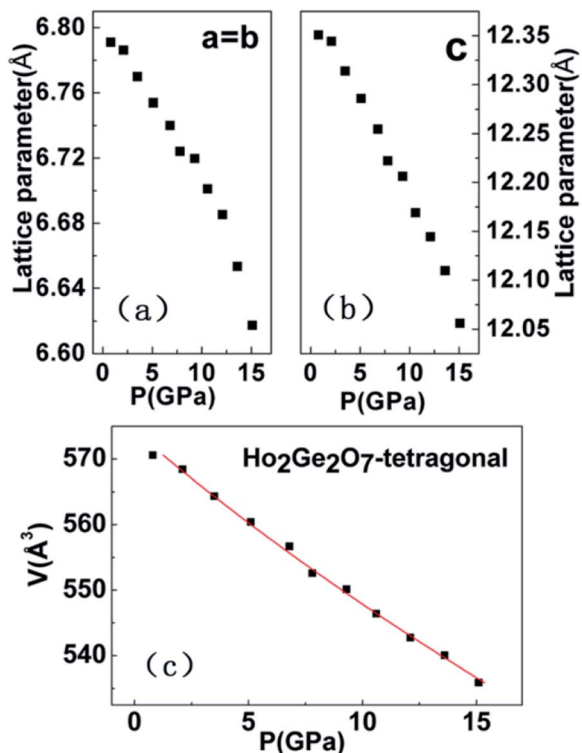
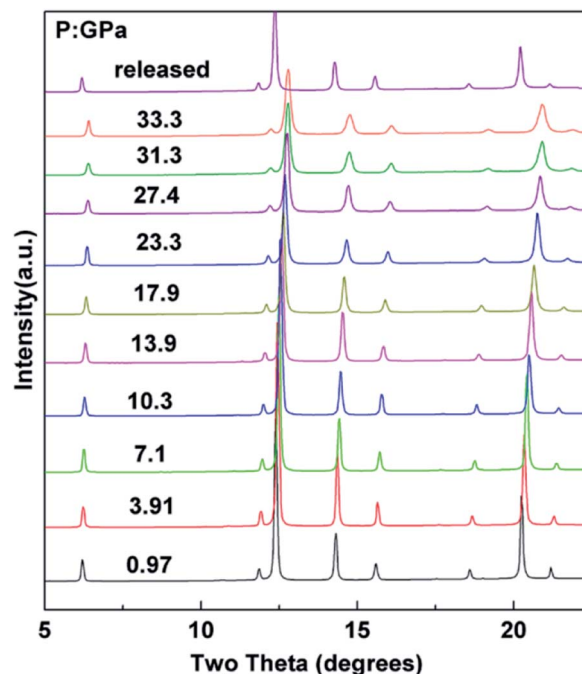Fig. 5 The lattice parameters ((a) and (b)) and unit cell volume (c) as a function of pressure for the tetragonal $Ho_2Ge_2O_7$.

Fig. 6 Selected XRD patterns of the cubic $Ho_2Ge_2O_7$ with increasing pressure. The cubic structure is stable up to 33.3 GPa.

induced amorphization, we can speculate that the tetragonal $Ho_2Ge_2O_7$ may become paramagnetic under high pressure.

The pressure dependences of the lattice parameters and volume of tetragonal $Ho_2Ge_2O_7$ up to 22.5 GPa are shown in Fig. 5. It is shown that the lattice parameters and volume of $Ho_2Ge_2O_7$ decrease smoothly with increasing pressure. In order to determine the bulk modulus B_0, its pressure derivative B_0', and the molar volume under ambient conditions V_0, the experimental pressure–volume data of the $Ho_2Ge_2O_7$ were fitted to a third-order Birch–Murnaghan equation of state (Fig. 5c).[33] The obtained bulk modulus B_0 is 193(4) GPa for the tetragonal phase with fixed $B_0' = 4$.

Structural stability of the cubic $Ho_2Ge_2O_7$ under high pressure

In situ XRD patterns of the cubic $Ho_2Ge_2O_7$ were collected up to 33.3 GPa at room temperature and the representative patterns are shown in Fig. 6. No splitting or extra peaks appear in the patterns, demonstrating that the cubic phase of the $Ho_2Ge_2O_7$ remains stable within the whole pressure range. In this ordered pyrochlore structure, all of the atoms are sited at defined positions, except for the O_{48f} atom. Hence, the degree of structural ordering can be determined by varying the x positional parameter of the O_{48f} atom. Previous studies on pyrochlore oxides have revealed that a sudden change of the x positional parameter of the O_{48f} atom occurred in the process of pressure-induced structural phase transition. For example, there was a rapid decrease of the x positional parameter with increasing pressure in $Gd_2Zr_2O_7$, implying a phase transition;[34]

the x-coordinate of the O_{48f} atom increased dramatically after the transformation in $Sm_2Zr_2O_7$.[35] From our refined results, the x parameter for the O_{48f} atom as a function of pressure, as shown in the inset of Fig. 7, does not exhibit any anomaly up to the highest pressure employed, indicating the structural stability of the cubic $Ho_2Ge_2O_7$. Recent experimental studies have reported that the pyrochlore $Ho_2Ge_2O_7$ exhibited all the distinctive properties of a dipolar spin ice: a small, positive Curie–Weiss constant; Pauling zero-point entropy; magnetization which saturated to half the magnetic moment; a spin-freezing transition in the ac susceptibility; and the characteristic magnetic diffuse scattering of spin ices.[19] The stability of
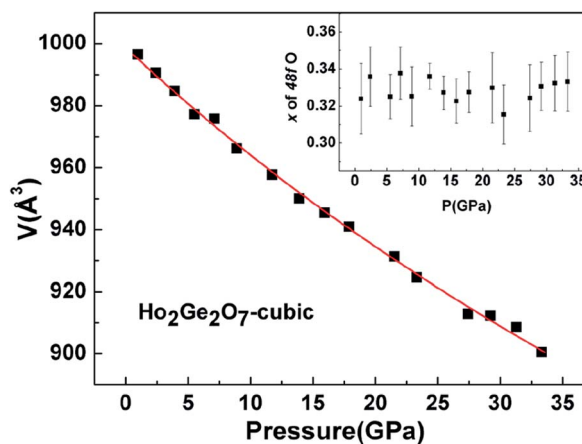

Fig. 7 Observed $P-V$ variation fitted with the third-order Birch–Murghnan (B–M) equation of state for the cubic $Ho_2Ge_2O_7$. The inset shows the pressure dependence of the x parameter for the O_{48f} atom.

the structure ensures the stability of these excellent properties under high pressure.

The pressure dependence of the unit cell volume of the cubic $Ho_2Ge_2O_7$ is shown in Fig. 7. The data are fitted by a third-order Birch–Murnaghan equation of state as is the case for the tetragonal $Ho_2Ge_2O_7$. The obtained bulk modulus B_0 is 263(4) GPa, quite a bit larger than for other ordered pyrochlore oxide materials. For example, the bulk moduli of $A_2Ti_2O_7$ (A = Ho, Y, Tb, Sm) were 213(2), 204(3), 199(1) and 164.8(1.5) GPa, respectively.[36,37] And also for $Gd_2Zr_2O_7$, the bulk modulus was 186(12) GPa.[34] By comparison, the hardness of the cubic phase in $Ho_2Ge_2O_7$ is higher than that of the tetragonal phase. The difference in bulk modulus might be due to the differences in structure and cohesive energy among these germanates.

4. Conclusions

In summary, the structural behaviors of two types of $Ho_2Ge_2O_7$ were studied under high pressure by *in situ* XRD measurements. Pressure-induced amorphization was found in the tetragonal $Ho_2Ge_2O_7$, which has a chain structure, and is suggested to be associated with the breaking-up of long chains of the edge-shared polyhedron group Ho_4O_{20}. By contrast, the cubic $Ho_2Ge_2O_7$ structure is stable at high pressures up to 33.3 GPa. The bulk modulus of the tetragonal $Ho_2Ge_2O_7$ was obtained as $B_0 = 193(4)$ GPa, and $B_0 = 263(4)$ GPa was obtained for the cubic phase.

Conflicts of interest

There are no conflicts to declare.

Acknowledgements

References

1 S. T. Bramwell and M. J. P. Gingras, *Science*, 2001, **294**, 1495–1501.

2 J. S. Gardner, M. J. P. Gingras and J. E. Greedan, *Rev. Mod. Phys.*, 2010, **82**, 53–107.

3 C. Castelnovo, R. Moessner and S. L. Sondhi, *Annu. Rev. Condens. Matter Phys.*, 2012, **3**, 35–55.

4 M. J. P. Gingras and P. A. McClarty, *Rep. Prog. Phys.*, 2014, **77**, 056501.

5 S. T. Bramwell, M. J. Harris, B. C. den Hertog, M. J. P. Gingras, J. S. Gardner, D. F. McMorrow, A. R. Wildes, A. L. Cornelius, J. D. M. Champion, R. G. Melko and T. Fennell, *Phys. Rev. Lett.*, 2001, **87**, 047205.

6 M. J. Harris, S. T. Bramwell, D. F. McMorrow, T. Zeiske and K. W. Godfrey, *Phys. Rev. Lett.*, 1997, **79**, 2554.

7 A. P. Ramirez, A. Hayashi, R. J. Cava, R. Siddharthan and B. S. Shastry, *Nature*, 1999, **399**, 333–335.

8 T. Fennell, O. A. Petrenko, B. Fåk, S. T. Bramwell, M. Enjalran, T. Yavors'kii, M. J. P. Gingras, R. G. Melko and G. Balakrishnan, *Phys. Rev. B: Condens. Matter Mater. Phys.*, 2004, **70**, 134408.

9 H. Kadowaki, Y. Ishii, K. Matsuhira and Y. Hinatsu, *Phys. Rev. B: Condens. Matter Mater. Phys.*, 2002, **65**, 144421.

10 K. Matsuhira, Y. Hinatsu, K. Tenya, H. Amitsuka and T. Sakakibara, *J. Phys. Soc. Jpn.*, 2002, **71**, 1576–1582.

11 H. D. Zhou, J. G. Cheng, A. M. Hallas, C. R. Wiebe, G. Li, L. Balicas, J. S. Zhou, J. B. Goodenough, J. S. Gardner and E. S. Choi, *Phys. Rev. Lett.*, 2012, **108**, 207206.

12 H. D. Zhou, S. T. Bramwell, J. G. Cheng, C. R. Wiebe, G. Li, L. Balicas, J. A. Bloxsom, H. J. Silverstein, J. S. Zhou, J. B. Goodenough and J. S. Gardner, *Nat. Commun.*, 2011, **2**, 478.

13 C. Castelnovo, R. Moessner and S. L. Sondhi, *Nature*, 2008, **451**, 42–45.

14 S. T. Bramwell, S. R. Giblin, S. Calder, R. Aldus, D. Prabhakaran and T. Fennell, *Nature*, 2009, **461**, 956–959.

15 L. D. C. Jaubert and P. C. W. Holdsworth, *Nat. Phys.*, 2009, **5**, 258–261.

16 D. J. P. Morris, D. A. Tennant, S. A. Grigera, B. Klemke, C. Castelnovo, R. Moessner, C. Czternasty, M. Meissner, K. C. Rule, J.-U. Hoffmann, K. Kiefer, S. Gerischer, D. Slobinsky and R. S. Perry, *Science*, 2009, **326**, 411–414.

17 T. Fennell, P. P. Deen, A. R. Wildes, K. Schmalzl, D. Prabhakaran, A. T. Boothroyd, R. J. Aldus, D. F. McMorrow and S. T. Bramwell, *Science*, 2009, **326**, 415–417.

18 S. R. Giblin, S. T. Bramwell, P. C. W. Holdsworth, D. Prabhakaran and I. Terry, *Nat. Phys.*, 2011, **7**, 252–258.

19 A. M. Hallas, J. A. M. Paddison, H. J. Silverstein, A. L. Goodwin, J. R. Stewart, A. R. Wildes, J. G. Cheng, J. S. Zhou, J. B. Goodenough, E. S. Choi, G. Ehlers, J. S. Gardner, C. R. Wiebe and H. D. Zhou, *Phys. Rev. B: Condens. Matter Mater. Phys.*, 2012, **86**, 134431.

20 S. Deemyad and J. S. Schilling, *Phys. Rev. Lett.*, 2003, **91**, 167001.

21 A. G. Gavriliuk, V. V. Struzhkin, I. S. Lyubutin, S. G. Ovchinnikov, M. Y. Hu and P. Chow, *Phys. Rev. B: Condens. Matter Mater. Phys.*, 2008, **77**, 155112.

22 I. Mirebeau, I. N. Goncharenko, P. Cadavez-Pares, S. T. Bramwell, M. J. P. Gingras and J. S. Gardner, *Nature*, 2002, **420**, 54–57.

23 H. K. Mao, J. Xu and P. M. Bell, *J. Geophys. Res.*, 1986, **91**, 4673–4676.

24 A. C. Larson and R. B. Von Dreele, *General Structure Analysis System*, LANSCE, MS-H805, Los Alamos, New Mexico, 1994.

25 E. G. Ponyatovsky and O. I. Barkalov, *Mater. Sci. Rep.*, 1992, **8**, 147–191.

26 A. V. Kolobov, J. Haines, A. Pradel, M. Ribes, P. Fons, J. Tominaga, C. Steimer, G. Aquilanti and S. Pascarelli, *Appl. Phys. Lett.*, 2007, **91**, 021911.

27 X. Q. Yan, W. J. Li, T. Goto and M. W. Chen, *Appl. Phys. Lett.*, 2006, **88**, 131905.

28 Z. X. Shen, C. W. Ong, S. H. Tang and M. H. Kuok, *J. Phys. Chem. Solids*, 1994, **55**, 665–669.

29 L. E. McNeil and M. Grimsditch, *Phys. Rev. Lett.*, 1992, **68**, 83–85.

30 C. Mead, R. J. Hemley and H. K. Mao, *Phys. Rev. Lett.*, 1992, **69**, 1387–1390.

31 Y. Li, R. Tang, N. Li, H. Li, X. Zhao, P. Zhu and X. Wang, *J. Appl. Phys.*, 2015, **118**, 035902.

32 E. Morosan, J. A. Fleitman, Q. Huang, J. W. Lynn, Y. Chen, X. Ke, M. L. Dahlberg, P. Schiffer, C. R. Craley and R. J. Cava, *Phys. Rev. B: Condens. Matter Mater. Phys.*, 2008, **77**, 224423.

33 F. Birch, *J. Geophys. Res.*, 1978, **83**, 1257–1268.

34 F. X. Zhang, J. Lian, U. Becker, R. C. Ewing, J. Hu and S. K. Saxena, *Phys. Rev. B: Condens. Matter Mater. Phys.*, 2007, **76**, 214104.

35 F. X. Zhang, J. Lian, U. Becker, L. W. Wang, J. Hu, S. K. Saxena and R. C. Ewing, *Chem. Phys. Lett.*, 2007, **441**, 216–220.

36 P. R. Scott, A. Midgley, O. Musaev, D. Muthu, S. Singh, R. Surya-narayanan, A. Revcolevschi, A. Sood and M. Kruger, *High Pressure Res.*, 2011, **31**, 219–227.

37 F. X. Zhang, B. Manoun, S. K. Saxena and C. S. Zha, *Appl. Phys. Lett.*, 2005, **86**, 181906.